Velocity distribution of the Milky Way satellites

T. Treial
Department of Physics, University of Surrey, Guildford, GU2 7XH, UK
E-mail address: tt00191@surrey.ac.uk, urn:6375357

The ΛCDM model describes the creation and the structure of the universe relatively well on large scales. It gives an explanation to the Cosmic Microwave Background, the abundancies of hydrogen & helium and the expansion of the universe. However it has challenges on the smaller scales, one of which is the velocity distribution of the Milky Way (MW) satellites. Compared to the simulations of Milky Way-like galaxies, observations predict larger tangential component than calculated. The aim for this report was to determine if the difference between the observations and simulations could be reduced by doing the error analysis more thoroughly – accounting for observational errors in the distance, radial velocity and proper motions to match the calculations with the measurements. Three sets of simulations were used – first including galaxies containing only dark matter haloes, another consisting a massive satellite (as the LMC near the MW) and the third one with the galaxy disc in the centre of the host. Different sets of simulations were considered to check if the additional bits of realism (e.g. the disk or the LMC) mattered in comparison with the previous analysis. In this paper the results from prior works were confirmed meaning that there was no significant difference between the observations taken earlier and the simulations. The error analysis did not improve the fit significantly hence the mismatch could mean that the simulations were missing something. After using updated velocities measured with the Gaia mission the mismatch between the measurements and simulations became minimal hence the problem appears to have been due to the observations all along.

Supervisor: D. Erkal

I. INTRODUCTION

A. Lambda-Cold Dark Matter (ΛCDM) model

Understanding how the universe formed was one of the biggest challenges amongst astronomers in the early 20th century. Several models were developed but today the leading model is called Lambda-Cold Dark Matter model (also called the standard model). It is said that the creation of a standard model of the universe was "one of the great success in physics" [1]. According to the theory, after the Big Bang, the universe was extremely hot and homogeneous but small fluctuations in density lead to the formation of dark matter clusters which started to glow and was the source for the cosmic microwave background (CMB) [2]. As the universe cooled the clumps of dark matter started to condense and the formation of stars and galaxies started. The model states the galaxies are created in dark matter haloes where small objects form first and over time these haloes consisting both dark and regular matter merge due to gravity to construct larger and larger galaxies observable today [2]. As of today the scientists have not yet experimentally verified the existence of dark matter but the astronomical procedures (e.g. galaxy rotation curves [3], gravitational-lensing measurements [4]) give important evidence for dark matter. From particle physics came new theories what dark matter could be made of – possible candidates for cold dark matter (CDM) are supersymmetric particles [5] or axions. [6] The other models classify the dark matter as hot (light neutrinos which are moving nearly the speed of light [7]) and warm (nonstandard gravitino [8] or more recently sterile neutrino [9] which interact with matter more weakly than neutrinos [7]) which can predict their distinctive velocities at some early time of the universe (e.g. at the epoch of recombination) [10].
The simulations using the ΛCDM model describe the large scale structure [2], cosmic microwave background [11] and the matter content of the universe [12] superbly. It also matches the abundancies

of the hydrogen and helium from the first moments after the Big Bang [13] and proves the expansion of the universe including using supernovae as standard candles [14]. In the simulations cold dark matter is described as a perfect and non-interacting pressureless liquid with zero speed of sound and viscosity. These characteristics make the N-body simulations significantly easier to model [7]. One good example is the Millennium simulation which was run in 2005 and used more than 10 billion clumps of dark matter, each modelled as a single particle with mass of billion solar masses to recreate the evolution of the matter distribution in a cubic region of the universe over 2 billion light-years on a side. After over a month, 25TB of data was output and the results were remarkable – the simulation recreated the homogeneous and isotropic appearance of the observable universe. As seen from Figure 1 the observation (blue) and simulation (red) regions are nearly identical in their statistical properties (e.g. the structure and the sizes of the filamentary appear similar). This result gave the astronomers a confirmation that the model had to be accurate on the great scales.

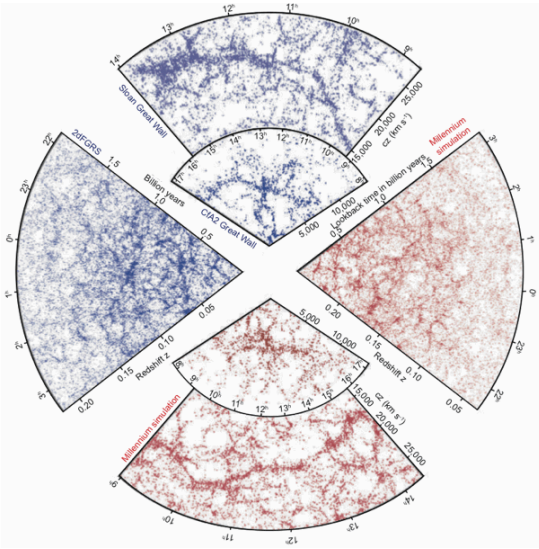

Figure 1. The comparison of the large scale structure of the universe between the observations (blue) and the Millennium simulation (red). Figure from Frenk et.al. (2012) [1].

Whilst the ΛCDM model works well on the large scales it has some challenges on the local regions. One of which is called the 'missing satellites' problem [15, 16]. While comparing the expectations of ΛCDM with observations is difficult, numerical simulations include far less "haloes orbiting within haloes" than can be observed [17]. One of the possible solutions for this problem is improving the spatial and mass resolution of the simulations to overcome the premature destruction of haloes (so-called 'overmerging' problem) [18]. When a galaxy and its dark matter halo interacts with a massive structure, the outskirts are stripped away by global tides and gravity but the central region survives and can be observed as a distinct structure within a cluster with its own dark matter halo [19]. Observations suggest this overmerging has been nearly complete on large scales however the MW contains only 11 of these massive satellites hence it was predicted the required mass resolution for the simulated haloes had to be ~10^8-10^9 $M_\odot$[1] to survive in galaxy groups and clusters [16, 20]. The high-resolution Adaptive Refinement Tree (ART) N-body calculations was run and it gave the results which were in reasonable agreement with the observations hence the problem was in the resolution of the simulations as predicted and that the fainter galaxies could not be detected yet [20].

By giving an answer to one problem, another one was created. It is known as the 'too big to fail' problem and it has similar mismatch between the number of observed and numerically calculated satellites [21]. It was found that the bulk of the most massive subhaloes in models are so massive and have a lot of dark matter that there is no reason why they will fail to form stars and be visible. In another words the observed satellites around MW are not massive enough to match with the computed ones [22]. The problem can be solved by modifying the simulation to be more realistic. The star formation starts the development of large fluctuations in the potential which can then lower the dark matter density. This leads to the different evolution of satellites and after falling into the MW potential, tidal stripping and shocks modify the mass distribution of both regular and dark matter even further. Using shallower density profiles and taking account tidal effects for modelling the results are consistent with the observations hence it could be one of the solutions for the problem [23].

[1] $M_\odot$(solar mass) = 1.98892x10^{30} kg [24]

B. Kinematics of the Milky Way satellites

This project concentrates mainly on the velocity distribution of the Milky Way satellites. One unexplained complication with ΛCDM model is the difference in the velocity scattering between the observations of the largest satellites of the MW and the numerical simulations [25]. The total velocity of a galactic body can be divided into two: radial and tangential components [26]. For example, if an object only has tangential velocity its orbit will be a perfect circle but the combination of the two velocity components make the orbit elliptical. Again, the difference between the observations and the simulations is the source of the problem - the numerical calculations have excessive radial velocity (v_{rad}) where the observed satellites predict more tangential orbits [25].

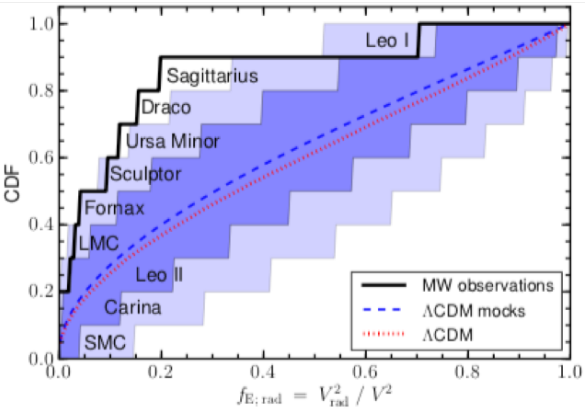

Figure 2. Cumulative distribution function[2] (CDF) for the velocity distribution fraction v_{rad}^2/v^2. Dashed blue line represents the computed values with errors, dotted red line shows the median of the simulations without observational errors. Solid black line shows the distribution for MW observations [27-35]. Darker and lighter shaded areas are the 1- and 2-σ scatter regions. Figure from Cautun & Frenk (2017) [25].

The previous work in [25] found the offset between the 10 MW satellites with measured proper motions and the modelled satellites (Figure 2). Only 1.5% of all simulated systems had the tangential velocity in the acceptable range as the measured data [27-35] plus they concluded that the mock observations were biased towards high v_{rad} values. In the paper, cosmological simulations from the Millennium II ΛCDM dark matter simulation [36, 37] were used. The authors found 3672 host haloes with range of stellar masses and for each host 10 most massive satellites were chosen. They used satellites more massive than 10^9 $M_\odot$ to make sure the simulations would start star formation in reality. Mock satellites within a distance of 300 kpc from the central galaxies were selected to make the analysis more accurate. To match the measurements with the simulations, 10 brightest satellites from the MW observations were selected as the velocity distribution was systematically biased between different catalogues [25].

To determine the errors, 1000 Monte Carlo realisations[3] were calculated for each simulation using the observational errors in the position and the proper motion. The uncertainties were sampled from the Gaussian distribution[4] centred on the most likely value of each quantity with dispersion equal to the error. After taking mock observations the coordinates were transformed from heliocentric to Galactocentric and plotted [25]. The shaded areas represented one- (darker) and two- (lighter) times standard deviation which meant that 68% and 95% of the calculated spread laid within that range respectively [38]. As seen from the Figure 2, in order to match simulations with observations extreme analytical values were needed. The authors discussed about the possible sources of errors and they believed that the LMC and the Small Magellanic Cloud (SMC) could have correlated orbital dynamics as the satellites are thought to have been accreted as a pair [39]. Moreover, measuring the proper motions of the satellites correctly is difficult hence it could possibly be affected by unknown systematic errors (i.e. the limited resolution and absence of baryonic effects for the cosmological models used). They proposed that more observations (e.g. from the Gaia mission) should be taken with more accurate equipment to reduce the errors in proper motions and perform similar tests for external galaxies to see if offset between the observations and calculations is similar to the Milky Way [25].

[2] Cumulative distribution function – probability that the variable takes a value less than or equal to x [40]
[3] Monte Carlo method – computational algorithm which rely on random sampling with many degrees of freedom [41]
[4] Gaussian distribution – continuous function which approximates the distribution of events and normalised such that the sum over all values of x gives a probability of 1 [42]

II. METHODS

A. Transformation of the coordinates

The position of a celestial object in the sky can be described in many ways. One popular method is to use Galactic coordinate system with the Sun in the centre. The position is defined in galactic longitude (l), which is measured by the eastward angle between the galactic centre and the observed body and latitude (b), which is the angle to north or south of the galactic equator as seen from Earth (Figure 3) [43]. The simulations provided contained 3D[5] positions, 3D velocities and the mass of each halo. As the Sun (or Earth, where the observations are taken) is not in the centre of the galaxy, the coordinates from the simulations had to be corrected for the position – (-8.3, 0, 0) kpc and the velocity – (11.1, 240, 7.3) km/s of the Sun [44].

The first step was to transform Cartesian coordinates to radius, r (distance between the satellite and the observations), and galactic coordinates, longitude, l, and latitude, b, using the transformations (Equation 1) [45]. In order to plot the velocity distribution fraction, 3D velocities had to be converted into radial velocity and proper motions[6] using Equations 2 & 3. U, V, W were defined as 3D velocity, v_r was the radial velocity, $\mu_l \cos b$ and μ_b were the proper motions and k represented a constant equal to 4.74047 (as the coordinates used were in kpc for distance, mas/yr for proper motions, and km/s for the velocities). To obtain the values for v_r and proper motions, the inverse of the M_{UVW} matrix had to be taken, which was simply its transpose (as it is defined as a rotational matrix) and multiplication between UVW and M_{UVW}^{-1} matrices was performed [44]. The results were divided by k and r respectively. After the values for radial velocity and proper motions were computed, the observational errors were added and sampled 100 times per

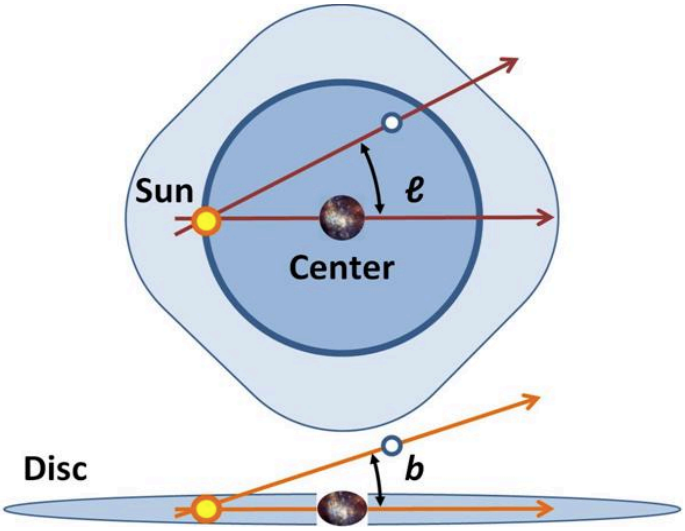

Figure 3. The definition of the galactic coordinates which uses the Sun as the origin. Longitude, l, is the angle along eastward direction and latitude, b, by north/south direction. Figure from Wikipedia [47].

$$\begin{pmatrix} r \\ l \\ b \end{pmatrix} = \begin{pmatrix} \sqrt{x^2 + y^2 + z^2} \\ \arctan\left(y/x\right) \\ \arccos\left(z/r\right) \end{pmatrix} \quad (1)$$

$$\begin{pmatrix} U \\ V \\ W \end{pmatrix} = M_{UVW} \begin{pmatrix} v_r \\ kr\mu_l \cos b \\ kr\mu_b \end{pmatrix} \quad (2)$$

$$M_{UVW} = \begin{pmatrix} \cos l \cos b & -\sin l & -\cos l \sin b \\ \sin l \cos b & \cos l & -\sin l \sin b \\ \sin b & 0 & \cos b \end{pmatrix} \quad (3)$$

$$v = \sqrt{U^2 + V^2 + W^2} \quad (4)$$

$$v_{rad} = \frac{U*x}{r} + \frac{V*y}{r} + \frac{W*z}{r} \quad (5)$$

[5] 3D position/velocity – Cartesian (X, Y, Z) coordinates [44]
[6] Proper motions – the apparent angular motion of a star/galaxy across the sky with respect to more distant stars [26]

simulation (Section 2.C). New values with errors were noted and transformed back to 3D velocities (U,V,W) to calculate total and radial velocity for plotting (Equation 4 & 5) [44].
Two sets of observational data were used – one from the Hubble Space Telescope (HST) and ground based observations [27-35] and another from Gaia mission [46]. The HST data was acquired from the Cautun & Frenk paper [25] using a software called DataThief [48] but the proper motions from Gaia mission were given in equatorial coordinates (μ_α, μ_δ) which had to be transformed to the 3D velocities using similar transformation matrices as stated in Equations 2 & 3. (Appendix A) [44]. The process of adding errors was repeated with the observational data and the velocity fractions were plotted for further analysis.

B. Raw simulations

In total, three sets of data were analysed in Python – dark matter halo (DMH), presence of the Large Magellanic Cloud (LMC) and with a regular matter disk in the centre of the host galaxy. The files were provided by Denis Erkal and as stated above they included 3D positions, 3D velocities and the mass of each sub-halo. They were cosmological simulations of Milky Way-like galaxies, similar to the Millennium run however at far higher resolution. The simulations included additional effects such as the presence of the LMC and the disk [44]. The work and analysis could be divided into three sub-sections.
Firstly, 10 simulations consisting only dark matter haloes were considered. DM-haloes are important nonlinear units of galactic structure and the foundation for galaxy creation. Understanding the basic properties of dark matter haloes is essential for improving ΛCDM model and learning how the galaxies are formed. Furthermore, the haloes are one of the best source for dark matter detection using direct (targeting dark matter particles within MW) or indirect (targeting the radiation from decaying dark matter particles) experiments which are strongly affected by the structure of haloes [1]. As stated above the coordinates were transformed and plotted to reproduce Figure 2 and check if it agrees with the results published in the previous paper. Similar to [25], haloes more massive than 10^9 $M_\odot$ were considered to secure the start of star formation and observability in reality and the satellites were selected within 300 kpc radius to the MW to improve the accuracy of the results[7].
Next, new set of 10 simulations containing a massive satellite were analysed. The data was selected to imitate more real-life like condition as the Large Magellanic Cloud (LMC) is orbiting the Milky Way [49]. The exact mass of the LMC is not known but the prediction states it is around $1/5^{th}$ of the mass of the MW [50] hence the presence of this large satellite would strongly perturb the kinematics of the MW and its satellites [51]. It is predicted the massive satellite has its own smaller satellites with very tangential orbits and the consequence is that the observed satellites have excessively tangential trajectories as well [52]. The simulations were not the exact reproductions of the MW but they were comparable and included a massive sub-halo. The aim was to compare this model with the observations and determine how the velocity distribution differ from the dark matter halo simulations.
Lastly, 10 simulations with a baryonic disk in the centre of the MW were studied. Including the disk to the simulations has been shown to play an important role in understanding the properties of the galactic satellites [53, 54]. The presence of the disk increases the central density of the host galaxy and it has been proven it can deplete the population of dwarf galaxies by several factors via tidal shredding [55]. Furthermore, several computational simulations have demonstrated that significant number of modelled satellites can be wiped out due to the coupling between the stellar feedback and the repeated battering by the disk shocks [56, 57]. In other words increased density has an effect of destroying satellites orbiting the host, especially the ones with large radial velocity [55]. The provided simulations were fundamentally identical to the dark matter halo simulations except they included the baryonic disk. Again the motivation behind using the set was to establish how it compares with the simulations run earlier.

[7] The same mass and radius limits were used for all three sets of simulations.

C. Error analysis

Determining the uncertainties and running mock observations was one of the essential part of this project. The errors were noted from the papers on the largest MW satellites [27-35] and the average, μ, and the standard deviation, σ, were calculated. The average observational errors in distance, r = 5.2468 kpc, radial velocity, v_{rad} = 9.18 km/s, and proper motions, μ_l = 0.0866 mas/yr & μ_b = 0.0873, from HST and ground based measurements were taken into account. For each variable new random value was generated from the Gaussian distribution, centred on the original simulation quantity with a dispersion σ. The code was looped 100 times to determine the spread from the curves with errors and calculate the average (i.e. the same Monte Carlo technique as used in Cautun & Frenk [25]). This method was useful as it allowed to take pseudo measurements without actually using the telescope. Additionally, the code was run several times with altered uncertainties – the errors in each variable were isolated (making the other errors negligible) to determine which one out of the three had the biggest effect. The code was run with e.g. doubled proper motion errors as well to ensure that the number generated was in the range of the "true" observation value and the systematic errors in the observations were taken to account (Figure 4). The new observational data was released recently and the values for proper motions changed in comparison with the old data hence by increasing the width of the Gaussian distribution it was confirmed the random sample laid the correct range. The code with different errors were run with all three sets of simulations and new velocity fractions were saved for plotting. For the next step, the average curve of the spread was calculated and the error-bars determined by selecting the exact width of the spread where 1-σ (~2/3) of the new curves were included (Figure 5). In total, 30 graphs were generated with the standard errors[8] (as there was 10 sets of files for each DMH, LMC and disk simulations). The same steps were completed by doubling the distance, radial velocity and proper motion errors, as well as isolating and making each one negligible. Thereafter, the median curve

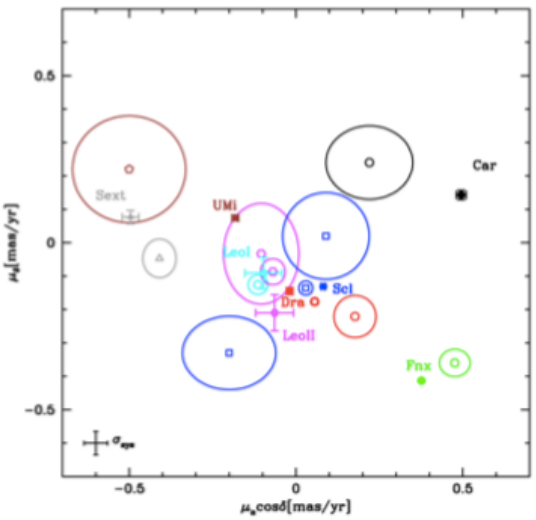

Figure 4. Proper motion comparison between the observations from Gaia mission (dots) and the literature values (circles) of the MW satellites. Symbols with the same colour represent the same sub-halo. Some of the satellites are quite far away from previous observations hence the measured values and errors from Gaia are considerably better. Figure from Helmi et.al. (2018) [46]

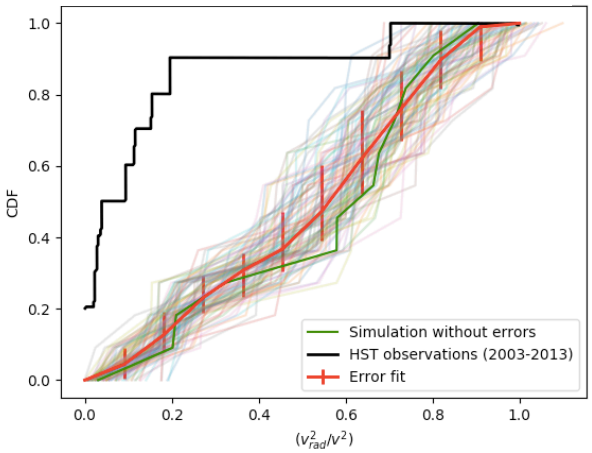

Figure 5. An example of the error analysis for the first file in dark matter halo simulation (no.1). Thick green line shows the velocity distribution from the original simulation (without added errors). The shaded lines were generated by adding the standard observational uncertainties and the solid red line is the average of the spread with the error-bars containing 1-σ of the spread. The black line represents the observational data from HST and ground based measurements. The calculated curves have higher v_{rad}^2/v^2 fractions than the measurements which are far more tangential (i.e. lower v_{rad}^2/v^2).

[8] Standard errors meaning that the average uncertainty in all variables taken to account

from 10 files was calculated with errors for each simulation and plotted to determine how the average line compares with the observations and other simulations. Finally, the errors were added to the measurements from the Gaia mission to determine the uncertainties for the observations and plotted for comparison.

III. RESULTS

The observational errors for the biggest satellites of the MW were noted for the radial velocity, distance and proper motions. The standard deviation was calculated for each variable to use it in error analysis to generate new random value from Gaussian distribution – σ_{v_rad} = 13.3037 km s^{-1}, σ_r = 2.5942 kpc, $\sigma_{\mu l}$ = 0.0631 mas yr^{-1}, $\sigma_{\mu b}$ = 0.0554 mas yr^{-1}.[9]

Firstly, the set consisting dark matter halo simulations were analysed. The errors were added to the code and 10 graphs were plotted. The results fluctuated quite a bit – as seen from Figure 5 both computed curves had relatively high radial velocity components but some simulations (e.g. Figure 6) had higher tangential velocities and matched the observational curve quite well. The new curves with errors were saved and the average of 10 simulations (and 100 runs within each one) was calculated. The result was similar to the one seen on Figure 9. This gave the conclusion that on average the simulations had a offset compared with the observations and further analysis had to be done.

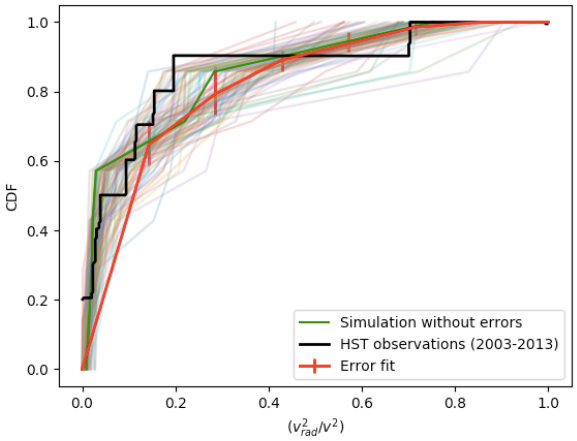

Figure 6. Dark matter simulation file no.8. The red (average) and the faint lines were computed with the standard observational errors. Green line was computed without errors, black curve represents the observational data from HST measurements. The figure shows that some of the simulations were consistent with the observations from HST.

The code was run and the average curves calculated with isolating each of the errors (e.g. error in distance, radial velocity or proper motion) as stated earlier to determine which had the largest effect on the results (Figure 7). As seen from the graph it was relatively difficult to determine how big of an influence isolating the errors had hence the curves were divided by the line with the standard

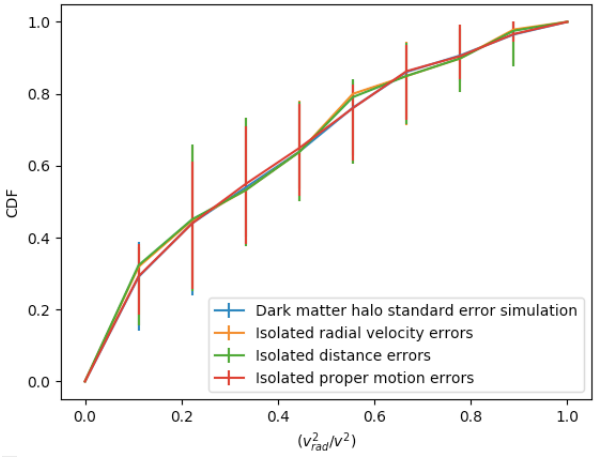

Figure 7. The average curves for DMH simulations with the error in one variable isolated.

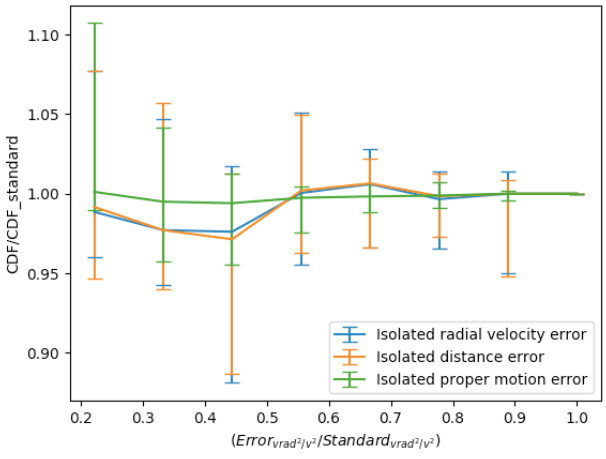

Figure 8. Comparison of errors for the average curves of DMH simulations. Isolated error lines were divided by the one with standard errors to cognise which error had the biggest effect.

[9] mas yr-1 – milliarcseconds per year and is the unit for the proper motion used

observational errors to make it easier to understand (Figure 8). Although the lines from different files fluctuated a lot as before on average isolating the errors did not make a big difference and surprisingly made the fit a bit more radial. The similar results were obtained with every set of errors (doubling, multiplying by 1.5 each variable separately and making each error negligible) – the different files within the set changed a lot but on average they did not make a big difference.

The same steps followed with the LMC and disk simulations. The same observational errors were added and similar analysis was completed. The results were similar to the ones above – different files within the set of simulations varied a lot but the mean curves from the simulations were mostly the same across all data as they fell in the same error range (Figure 9). The mismatch between the HST observations and the simulations used was confirmed however after calculating the velocity fractions from the Gaia mission the difference between the simulations and observations became minimal. The median lines still were not equal but the calculated errors had a relatively good match hence this could be one of the solutions for the velocity distribution problem – the simulations were correct from the beginning but the misalignment became from the observational data.

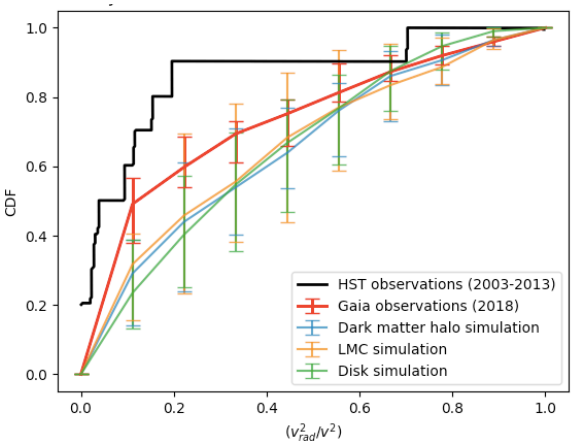

Figure 9. Velocity distribution between the DMH, LMC & disk simulations and HST & Gaia observations. The error-bars represent the 1-σ uncertainty. The graph shows the comparison between each simulation used and the improved fit between the simulations and new observations from Gaia mission.

As stated, different files within the simulations fluctuated a lot – some had high radial velocity components (Figure 5) but others were fairly observation-like (Figure 6). This raised a question why did the different files had such diverse velocity fractions? The prediction from Denis Erkal was that it might have been something to do with the positions and distances of the satellites in each simulation. The satellites further away might have had larger tangential velocity components than observed as naturally it is more difficult to define the correct values for the bodies further away and it could have had a larger effect on the satellites further away (i.e. the large proper motion errors make the satellites appear tangential) [25]. Moreover, as the mock observations were not taken in the centre of the galaxy the radial and tangential velocity components could have been swapped by definition – the radial and tangential velocities as observed from the Sun do not necessarily correspond to the radial and tangential

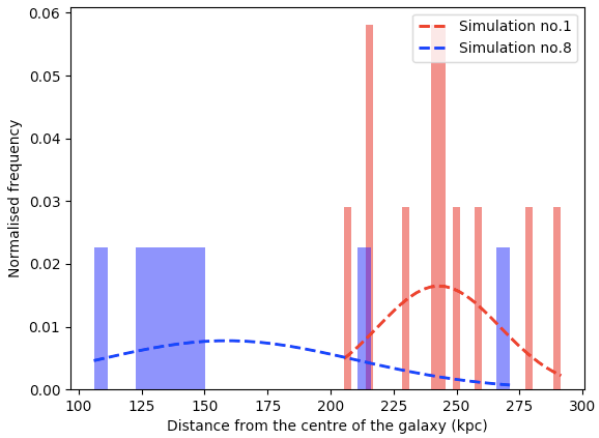

Figure 10. The distances of satellites from the centre of the simulated host galaxy for DMH simulation files no.1 (Figure 5, red) and no.8 (Figure 6, blue). The curve represents the normalised probability density function.

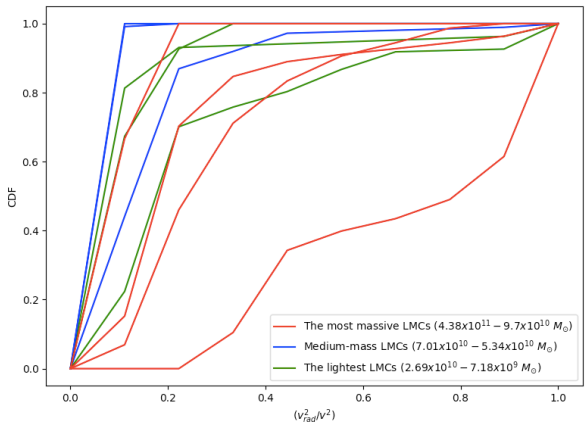

Figure 11. Velocity distribution of the largest satellites from LMC simulation. The red lines represent the most massive, blue lines are the mid-range and green line denotes the lightest satellites.

velocities with respect to the centre of the MW. In order to test it, the distances were plotted from the centre of the MW as a histogram to see if the distance had any effect on the velocity distribution (Figure 10). The graph indicated the distances of the satellites from Figure 5 and Figure 6 which had the most radial and tangential orbits respectively. As seen from Figure 10, the simulation number 1 consisted of satellites further away than in the simulation number 8. The equivalent results were observed for the LMC and disk simulations as well hence there was a clear dependence between the distances and the velocity distributions. It warrants further study since the distance of the satellites appears to be significant and should be taken into account for additional projects.
The effect of the LMC was also reviewed. The hypothesis was that the LMC has mostly tangential orbit and maybe the mass of the satellite shifts the velocity fractions. In order to check the theory, the velocity distributions of the most massive satellites from the simulations were plotted separately (Figure 11). The sub-haloes were divided into three groups – 3 the lightest, 3 mid-range & 4 the most massive and the motive was to determine if the mass of a halo had any effect on the velocity fraction. The results showed that there was not a clear trend between the mass of the halo and the velocity component. On average the orbits were more tangential as expected but the velocity distribution fluctuated between the satellites with different mass hence the hypothesis could not be confirmed.

IV. CONCLUSIONS

The ΛCDM model describes the structure of the universe very well on the large scales but it has some issues on smaller scales. One of which is the velocity distribution of the Milky Way satellites. The previous work was done by Cautun & Frenk [25] who found the offset between the ΛCDM model simulations and Hubble Space Telescope and ground based observations. They noticed that the simulations have excessive radial velocity whereas observations predict more tangential orbits. The authors predicted that the source of the mismatch could be in the simulations as the model used did not take account the presence of a massive satellite or baryonic effects. In this report three different sets of simulations containing 10 simulations were used – one with satellites containing dark matter haloes, second with the presence of a massive satellite (similar as the LMC to the MW) and finally one with baryonic disk in the centre of the host to understand how different simulations compare with the measurements. Another goal for this project was to perform the error analysis more thoroughly – the observational errors in radial velocity, distance and proper motions were taken into account to determine how they change the velocity fraction. Furthermore, the errors were altered to see which affects the results the most.
The results were unexpected – on average the different simulations and diverse uncertainties did not change the velocity distribution significantly. The mismatch between the simulations used and the HST observations was confirmed but after analysing the new observational data from the Gaia mission the gap between the measurements and calculations became minimal. Specifically, it could mean that the numerical predictions were correct all along and the observations were inaccurate. The results from this paper give confidence that ΛCDM model is the correct method explaining the structure of the universe even on the local scales.
For further studies, another set of simulations could be analysed with the presence of both the LMC and the baryonic disk to establish if the fit would improve even further. Additionally, more time could be taken to analyse simulations, e.g. determine how the distance between the host and satellites change the velocity distribution throughout all simulations and if the results would be biased or show the velocity fractions between the heavier and lighter satellites with a presence of a disk to understand how the situation changes the outcome. As stated in the paper from Cautun & Frenk [25] the similar analysis could be made with external galaxies to confirm the same result throughout the universe. In order to do that, better equipment is needed to measure the proper motions for fainter galaxies further away more accurately.

V. ACKNOWLEDGEMENTS

I would like to thank Dr. Denis Erkal for giving me this opportunity to work on this project. The process throughout the semester was really enjoyable and I learned a lot starting from basic computing in Python

and ending with understanding & analysing different graphs. The tasks given were clear each week and I think the structure for the assignment was thought through well. The feedback was always quick and positive and I think this was one of the reasons I was able to complete the project so smoothly.

APPENDIX A

The transformation matrix for converting the equatorial coordinates into 3D velocities [45]. This was used to plot the velocity distribution for the new observational data from the Gaia mission. U, V, W represent the 3D velocities, A'_G is the transpose of A_G matrix and r is the distance, v_r is the radial velocity, $\mu_\alpha cos\delta$ & μ_δ are the proper motion measured in equatorial coordinates. Constant k = 4.74047 [44].

$$\begin{pmatrix} U \\ V \\ W \end{pmatrix} = A'_G M_{UVW} \begin{pmatrix} v_r \\ kr\mu_\alpha cos\delta \\ kr\mu_\delta \end{pmatrix} \tag{6}$$

$$A_G = \begin{pmatrix} -0.0548755604 & 0.4941094279 & -0.8676661490 \\ -0.8734370902 & -0.4448296300 & -0.1980763734 \\ -0.4838350155 & 0.7469822445 & 0.4559837762 \end{pmatrix} \tag{7}$$

$$M_{UVW} = \begin{pmatrix} cos\alpha\ cos\delta & -sin\alpha & -cos\alpha\ sin\delta \\ sin\alpha\ cos\delta & cos\alpha & -sin\alpha\ sin\delta \\ sin\delta & 0 & cos\delta \end{pmatrix} \tag{8}$$

[1] C.S. Frenk and S.D.M. White, Dark matter and cosmic structure, Ann. Phys. **524**, 507 (2012).

[2] R.J. GaBany, The Formation and Evolution of Galaxies, http://www.cosmotography.com/images/galaxy_formation_and_evolution.html, retrieved 12/05/2018.

[3] M. Persic et.al., The universal rotation curve of spiral galaxies – I. The dark matter connection, Monthly Notices of the Royal Astronomical Society, **281**, 1, pp.27-47 (1996).

[4] A.T. Lefor and T. Futamase, Comparison of Strong Gravitational Lens Model Software I. Time delay and mass calculations are sensitive to changes in redshift and are model dependent, arXiv:1307.4600v1 (2013).

[5] J. Ellis et. al., Supersymmetric relics from the big bang, Nucl. Phys. B **238**, pp. 453-476 (1984).

[6] J. Preskill, M.B. Wise and F. Wilczek, Cosmology of the invisible axion, Phys. Lett. B **120**, pp. 127-132 (1983).

[7] D.B. Thomas et.al., Constraining Dark Matter Properties With Cosmic Microwave Background Observations, arXiv:1601.05097v2 (2016).

[8] G.R. Blumenthal, H. Pagels and J.R, Primack, Galaxy formation by dissipationless particles heavier than neutrinos, Nature, **299**, 37 (1980).

[9] M. Shaposhnikov, Sterile neutrinos in cosmology and how to find them in the lab, J. Phys. Conf. Ser. **136**, 022045 (2008).

[10] J.R. Bond, G. Efstathiou and J. Silk, Massive Neutrinos and the Large-Scale Structure of the Universe, Phys. Rev. Lett. **45**, pp. 1980-1984 (1980).

[11] Planck Collabration et al., Planck 2015 results. XIII. Cosmological parameters, A&A. **594**, A13 (2016).

[12] H. Gil-Marín et.al., The clustering of galaxies in the completed SDSS-III Baryon Oscillation Spectroscopic Survey: Cosmological implications of the Fourier space wedges of the final sample, arXiv:1607.03143v2 (2016).

[13] S.F. Anderson et.al., The Eighth Data Release Of The Sloan Digital Sky Survey: First Data From SDSS-III, The American Astronomical Society, **193**, 29, pp.17 (2011).
[14] A.G. Riess et.al., Is There An Indication Of Evolution Of Type Ia Supernovae From Their Rise Times?, The American Astronomical Society, **118**, pp.2668-2674 (1999).
[15] A. Klypin et.al., Where Are the Missing Galactic Satellites?, The Astrophysical Journal, **522**, 1, pp. 82-92 (1999).
[16] B. Moore et.al., Dark Matter Substructure within Galactic Halos, The Astrophysical Journal, **524**, 1, pp. L19-L22 (1999).
[17] N. Katz, S.D.M. White, Hierarchical galaxy formation - Overmerging and the formation of an X-ray cluster, The Astrophysical Journal, Part 1. **412**, 2, pp.455-478 (1993).
[18] B. Moore et.al., On the Destruction and Overmerging of Dark Halos in Dissipationless N-Body Simulations, The Astrophysical Journal, **457**, pp. 455 (1996).
[19] P. Natarajan et.al., The Mass-to-Light Ratio of Early-Type Galaxies: Constraints from Gravitational Lensing in the Rich Cluster AC 114, The Astrophysical Journal, 499, 2, pp. 600-607 (1998).
[20] A. Klypin et.al., Galaxies in N-Body Simulations: Overcoming the Overmerging Problem, The Astrophysical Journal, 516, pp. 530-551 (1999).
[21] M. Boylan-Kolchin, J.S. Bullock and M. Kaplinghat, Too big to fail? The puzzling darkness of massive Milky Way subhaloes, Mon. Not. Roy. Astron. Soc. 415, pp. L40 (2011).
[22] S. Kohler, A Solution to "Too Big to Fail", AAS Nova Highlight, Id.1563 (2016).
[23] M. Tomozeiu, T. Quinn and L. Mayer, Tidal Stirring Of Satellites With Shallow Density Profiles Prevents Them From Being Too Big To Fail, The Astrophysical Journal Letters, **827**, 1, pp. 7 (2016).
[24] Astronomical Constants, http://asa.usno.navy.mil/static/files/2014/Astronomical_Constants_2014.pdf, retrieved 13/05/2018.
[25] M. Cautun and C.S. Frenk, The tangential velocity excess of the Milky Way satellites, arXiv:1612.01529 (2016).
[26] R. Pogge, Introduction to Stars, Galaxies, & the Universe. Lecture 6: The Motion of the Stars, http://www.astronomy.ohio-state.edu/~pogge/Ast162/Unit1/motions.html, retrieved 13/05/2018.
[27] C. Pryor et.al., Proper Motion of the Sagittarius Dwarf Galaxy Based on Hubble Space Telescope Imaging, The Astronomical Journal, 139, pp. 839-856 (2010).
[28] N. Kallivayalil et.al., Third-epoch Magellanic Cloud Proper Motions. I. Hubble Space Telescope/WFC3 Data and Orbit Implications, The Astrophysical Journal, **764**, 2, pp. 24 (2013).
[29] C. Pryor et.al., Proper Motion of the Draco Dwarf Galaxy Based on Hubble Space Telescope Imaging, The Astronomical Journal, **149**, 42, pp. 12 (2015).
[30] S. Piatek et.al., Proper Motions of Dwarf Spheroidal Galaxies from Hubble Space Telescope Imaging. IV. Measurement for Sculptor, The Astronomical Journal, **131**, pp. 1445-1460 (2006).
[31] S. Piatek et.al., Proper Motions of Dwarf Spheroidal Galaxies from Hubble Space Telescope Imaging. III. Measurement for Ursa Minor, The Astronomical Journal, **130**, 1, pp. 95-115 (2005).
[32] S. Piatek et.al., Proper Motions of Dwarf Spheroidal Galaxies from Hubble Space Telescope Imaging. II. Measurement for Carina, The Astronomical Journal, **126**, 5, pp. 2346-2361 (2003).
[33] S. Piatek et.al., Proper Motions of Dwarf Spheroidal Galaxies from Hubble Space Telescope Imaging. V. Final Measurement for Fornax, The Astronomical Journal, 133, 3, pp. 818-844 (2007).
[34] S. Piatek et.al., Proper Motion of the Leo II Dwarf Galaxy Based On Hubble Space Telescope Imaging, The Astronomical Journal, **152**, 6, pp.15 (2016).
[35] S.T. Sohn et.al., The Space Motion of Leo I: Hubble Space Telescope Proper Motion and Implied Orbit, The Astronomical Journal, 768, 2, pp. 21 (2013).
[36] M. Boylan-Kolchin et.al., Resolving cosminc structure formation with the Millenium-II Simulation, Monthly Notices of the Royal Astronomical Society, 398, 3, pp. 1150-1164 (2009).
[37] S.J. Clay et.al., Galaxy formation in the Planck cosmology – III. The high-redshift universe, Monthly Notices of the Royal Astronomical Society, **451**, pp. 2692-2702 (2015).

[38] J.M. Bland et.al., Statistics notes: Measurement error, BMJ 1996;312:1654 (1996).
[39] G. Besla et.al., The role of dwarf galaxy interactions in shaping the Magellanic System and implications for Magellanic Irregulars, Monthly Notices of the Royal Astronomical Society, **421**, pp. 2109-2138 (2012).
[40] D. Zwillinger and S. Kokoska, Standard probability and Statistics tables and formulae, CRC Press, page 49 (2010).
[41] D.P. Kroese et.al., Why the Monte Carlo method is so important today, Wiley Online Library, **6**, 6, pp. 386-392 (2014).
[42] J.W. Rohlf, Modern Physics from alpha to Z0, Wiley (1994).
[43] A. Blaauw et.al., The new IAU system of galactic coordinates, Monthly Notices of the Royal Astronomical Society, **121**, 2, pp. 123 (1960).
[44] E.W. Weisstein, Spherical Coordinates, http://mathworld.wolfram.com/SphericalCoordinates.html, retrieved 14/05/2018.
[45] D. Erkal et.al., Notes on proper motions, Private collection (2018).
[46] A. Helmi et.al., Gaia Data Release 2: Kinematics of globular clusters and dwarf galaxies around the Milky Way, arXiv:1804.09381v1 (2018).
[47] https://en.wikipedia.org/wiki/Galactic_coordinate_system#/media/File:Galactic_coordinates.JPG, retrieved 13/05/2018.
[48] https://datathief.org/, retrieved 20/04/2018.
[49] G. Shattow et.al., Implications of recent measurements of the Milky Way rotation for the orbit of t, Monthly Notices of the Royal Astronomical Society, **392**, L21 (2009).
[50] X.X. Xue et.al., The Milky Way's Circular Velocity Curve to 60 kpc and an Estimate of the Dark Matter Halo Mass from Kinematics of ~2400 SDSS Blue Horizontal Branch Stars, Astrophys. J. 684, pp. 1143-1158 (2008).
[51] F.A. Gomez et.al., And Yet It Moves: The Dangers Of Artificially Fixing The Milky Way Center Of Mass In The Presence Of A Massive Large Magellanic Cloud, The Astrophysical Journal, **802**, 2, pp. 16 (2015).
[52] J. Peñarrubia et.al., A timing constraint on the (total) mass of the Large Magellanic Cloud, arXiv:1507.03594 (2015).
[53] J. Peñarrubia et.al., The impact of dark matter cusps and cores on the satellite galaxy population around spiral galaxies, Monthly Notices of the Royal Astronomical Society, **406**, 2, pp. 1290-1305 (2010).
[54] E. D'Ongia et.al., Substructure Depletion on the Milky Way Halo by the Disk, The American Astronomical Society, **709**, 2, pp. 1138-1147 (2010).
[55] P. Jetwa, D. Erkal and V. Belokurow, The upper bound on the lowest mass halo, arXiv:1612.07834 (2017).
[56] S. Geen, A. Slyz and J. Devriendt, Satellite survival in highly resolved Milky Wasy class haloes, Monthly Ntices of the Royal Astronomical Society, **429**, 1, pp. 633-651 (2013).
[57] A.M. Brooks and A. Zolotov, Why Baryons Matter: The Kinematics of Dwarf Spheroidal Satellites, The Astrophysical Journal, **786**, pp.87 (2014).